LETTER

doi:10.1038/nature10309

Perpendicular switching of a single ferromagnetic layer induced by in-plane current injection

Ioan Mihai Miron[1], Kevin Garello[1], Gilles Gaudin[2], Pierre-Jean Zermatten[2], Marius V. Costache[1], Stéphane Auffret[2], Sébastien Bandiera[2], Bernard Rodmacq[2], Alain Schuhl[2] & Pietro Gambardella[1,3,4]

Modern computing technology is based on writing, storing and retrieving information encoded as magnetic bits. Although the giant magnetoresistance effect has improved the electrical read out of memory elements, magnetic writing remains the object of major research efforts[1]. Despite several reports of methods to reverse the polarity of nanosized magnets by means of local electric fields[2,3] and currents[4–6], the simple reversal of a high-coercivity, single-layer ferromagnet remains a challenge. Materials with large coercivity and perpendicular magnetic anisotropy represent the mainstay of data storage media, owing to their ability to retain a stable magnetization state over long periods of time and their amenability to miniaturization[7]. However, the same anisotropy properties that make a material attractive for storage also make it hard to write to[8]. Here we demonstrate switching of a perpendicularly magnetized cobalt dot driven by in-plane current injection at room temperature. Our device is composed of a thin cobalt layer with strong perpendicular anisotropy and Rashba interaction induced by asymmetric platinum and AlO_x interface layers[9,10]. The effective switching field is orthogonal to the direction of the magnetization and to the Rashba field. The symmetry of the switching field is consistent with the spin accumulation induced by the Rashba interaction and the spin-dependent mobility observed in non-magnetic semiconductors[11,12], as well as with the torque induced by the spin Hall effect in the platinum layer[13,14]. Our measurements indicate that the switching efficiency increases with the magnetic anisotropy of the cobalt layer and the oxidation of the aluminium layer, which is uppermost, suggesting that the Rashba interaction has a key role in the reversal mechanism. To prove the potential of in-plane current switching for spintronic applications, we construct a reprogrammable magnetic switch that can be integrated into non-volatile memory and logic architectures. This device is simple, scalable and compatible with present-day magnetic recording technology.

The coupling of spin and orbital angular momenta underlies the magnetic anisotropy properties of ferromagnets. Strong anisotropy allows for permanent, stable storage but also requires stronger magnetic fields to write information to magnetic media. An ideal solution to this problem requires the spin–orbit interaction to be beneficial for both storage and writing purposes. Experiments on non-magnetic semiconductors have revived interest in effective magnetic fields originating in spin–orbit coupling[11,15–20]. Such fields relate the spin of an electron to its momentum, converting a charge current into a source of spin polarization even in the absence of magnetism. More recently, spin–orbit fields have been predicted[21,22] and observed in ferromagnets lacking structural inversion symmetry[6,9], where the *s*–*d* exchange interaction between charge carriers and localized *d* electrons mediates the effect of the spin–orbit fields on the magnetization. The possibility of generating strong spin–orbit fields in ferromagnetic metals (FMMs) is particularly interesting for applications, owing to the robust Curie temperature and perpendicular magnetic anisotropy (PMA) afforded by such systems. So far, however, the centrosymmetric lattice properties of FMMs restrict this possibility to generation of the Rashba effect[23], as inversion asymmetry can only be achieved by sandwiching an FMM layer between two dissimilar interfaces, one of which is usually a heavy, non-magnetic element[9,24]. Owing to the Rashba interaction, electrons flowing in the plane of a conductor with asymmetric interfaces experience an effective magnetic field $\mathbf{B}_R = \alpha_R(\hat{\mathbf{z}} \times \mathbf{j})$, where α_R is the Rashba constant, $\hat{\mathbf{z}}$ is a unit vector along the perpendicular axis (the z direction) and $\mathbf{j}$ is the vector current density. As the interface effects responsible for the Rashba interaction also induce PMA, $\mathbf{B}_R$ is orthogonal to the easy magnetization axis. Therefore, the Rashba field by itself cannot be used to control magnetization reversal in FMMs[9].

Here we demonstrate up–down magnetic switching of a cobalt dot characterized by strong PMA and Rashba interaction induced by an in-plane current. Bipolar reversal of the magnetization is achieved by injecting in-plane current pulses of either positive or negative sign parallel to a static magnetic field of moderate amplitude. This effect is discussed in terms of the symmetry of the current-induced spin–orbit fields acting on the cobalt layer. Switching occurs in single-layer FMMs independently of the domain configuration of the sample and without the need for a polarizer layer. We show that this phenomenon leads to innovative device architectures for spintronics.

Each of our samples consists of a 500 nm × 500 nm cobalt dot sandwiched between a 3-nm-thick platinum layer (below) and a 1.6-nm-thick AlO_x cap (above; Fig. 1a). The thickness of the cobalt layer is chosen to be 0.6 nm to maximize the Rashba effect due to structure inversion asymmetry at the platinum and AlO_x interfaces[9]. The AlO_x and cobalt layers are each patterned into a square dot, whereas the platinum layer is etched into a cross-shaped structure for current injection and Hall voltage measurements. The perpendicular magnetization of the dot, M_z, is measured in terms of the anomalous Hall resistance, which varies by $R_{Hall} = 0.8\,\Omega$ for opposite orientations of M_z. A rotating sample stage is used to apply an external magnetic field, $\mathbf{B}$, at polar and azimuthal angles θ and ϕ (Fig. 1a). To study the effects of an electric current on M_z, we apply 15-ns-long pulses of variable amplitude supplied by a voltage generator, using the circuit shown in Fig. 1b. All measurements are performed at room temperature.

The central result of this work is shown in Fig. 1c, d, where we compare field-induced and current-induced reversal of M_z. We first perform a standard magnetization measurement in the absence of current pulses, recording M_z during a single sweep of $\mathbf{B}$ applied parallel to the current injection line (Fig. 1c, solid line). The field is intentionally tilted off-plane by 2° ($\theta = 92°$, $\phi = 0°$) to prevent the formation of magnetic domains. Magnetization reversal occurs at the coercive field $|B_c| = 300$ mT, owing to the residual component, B_z, parallel to the out-of-plane easy axis of the dot. We then repeat this magnetic field sweep, but stop at each value of B and inject a positive (set) current pulse and negative (reset) current pulse, measuring M_z after each pulse. The black and red points (Fig. 1d) indicate the orientation of M_z after the alternating injection of set and reset pulses of amplitude

[1]Catalan Institute of Nanotechnology (ICN-CIN2), E-08193 Barcelona, Spain. [2]SPINTEC, UMR-8191, CEA/CNRS/UJF/GINP, INAC, F-38054 Grenoble, France. [3]Departament de Física, Universitat Autonoma de Barcelona, E-08193 Barcelona, Spain. [4]Institució Catalana de Recerca i Estudis Avançats (ICREA), E-08010 Barcelona, Spain.

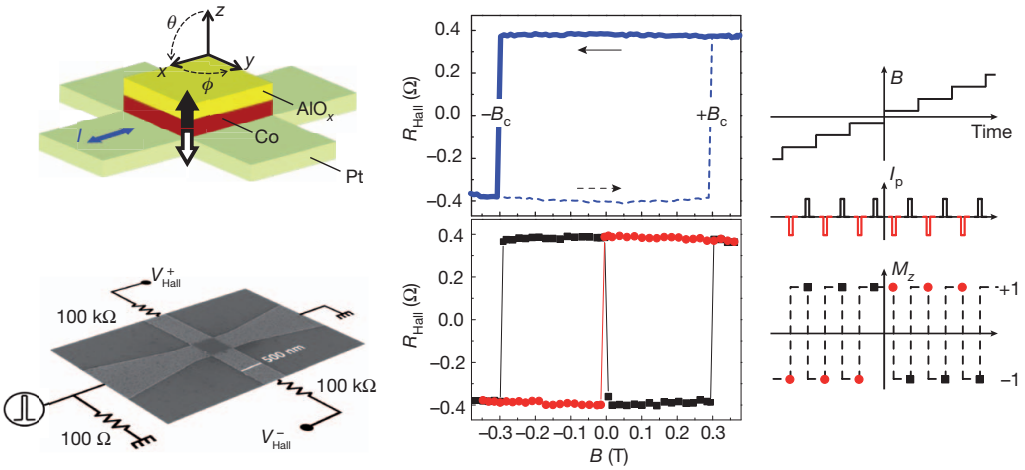

Figure 1 | Device schematic and current-induced switching. **a**, Hall cross geometry. Black and white arrows indicate the 'up' and 'down' equilibrium magnetization states of the cobalt layer, respectively. **b**, Scanning electron micrograph of the sample and electric circuitry used in the measurements. V^+_{Hall} and V^-_{Hall} represent the two terminals for the Hall voltage measurements. **c**, M_z measured by the anomalous Hall resistance as a function of applied field, B. **d**, M_z measured after the injection of positive (black squares) and negative (red circles) current pulses of amplitude $I_p = 2.58$ mA. The data are reported during a single sweep of B, corresponding to the solid line in **c**. **e**, Schematic of the pulse sequence and magnetization measurements. In both **c** and **d**, B is applied at $\theta = 92°$, parallel to the current direction ($\phi = 0°$). The 2° offset with respect to the ideal in-plane direction is used to define the residual component B_z unambiguously.

$I_p = 2.6$ mA. This plot shows two striking effects, illustrated in Fig. 1e. First, black and red points that represent magnetizations of opposite sign indicate switching of M_z from up to down and vice versa following every pulse of current. Second, the sense of switching reverses as B goes through zero. Positive and negative sweeps of B give identical results. We note that pulse-induced magnetization reversal occurs in the entire bistability range of the FMM delimited by B_c, down to $B \approx 5$ mT. This behaviour is independent of the domain configuration of the sample (Supplementary Information) and is remarkably different from that expected for known magnetic interactions. For example, the in-plane Rashba and Oersted fields, as well as Joule heating, would tend to favour a demagnetized state that is not compatible with the observed deterministic switching[9], whereas precessional switching does not depend on the current direction[25].

Measurements performed over a range of currents offer further insight into the switching phenomenon (Fig. 2). Although weak current pulses have no effect, starting at around $I_p = 1.3$ mA (Fig. 2a) we observe a gradual reduction in the coercive field (Fig. 2c, red triangles). This behaviour can be understood by noting that the combination of a weak current-induced effect and the residual component B_z assists magnetization reversal towards the equilibrium direction, parallel to B_z. At $I_p \approx 1.9$ mA, however, we observe the onset of current-induced

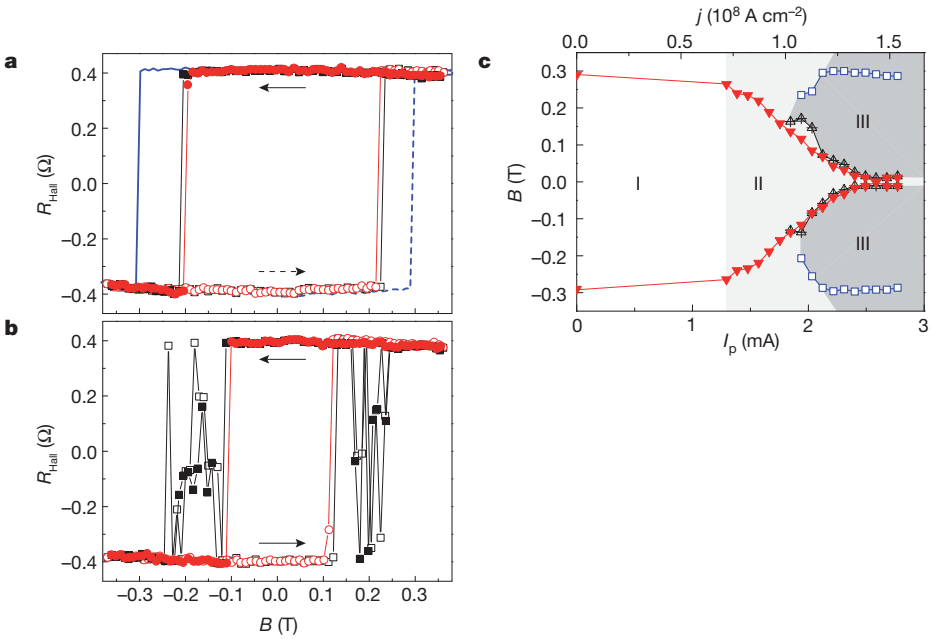

Figure 2 | Switching efficiency as a function of current amplitude. **a**, **b**, M_z measured after injection of positive (black squares) and negative (red circles) current pulses of amplitude $I_p = 1.57$ mA (**a**) and $I_p = 1.94$ mA (**b**). Filled symbols indicate data recorded during a $+B \rightarrow -B$ sweep and open symbols indicate data recorded during a $-B \rightarrow +B$ sweep, as shown by the arrows. The solid and dashed lines in **a** represent M_z as a function of field. **c**, Switching efficiency as a function of pulse amplitude and applied magnetic field. Region I: conventional field-induced magnetization reversal occurs at $B = B_c$. Region II: assisted reversal. Red triangles indicate the minimum external field required to reverse M_z parallel to B_z. Region III: pulse-induced switching. Black triangles indicate the minimum field at which positive current pulses reverse the magnetization antiparallel to B_z. The maximum field at which switching is observed (blue open squares) coincides with the coercivity of the dot.

switching events (Fig. 2b), which become systematic as I_p is further increased above 2.3 mA (Fig. 1d). The high-field switching limit (Fig. 2c, blue squares) gradually extends up to $B = B_c$, indicating that the torque working against the action of B_z becomes stronger as I_P increases. At the same time, the minimum in-plane field component necessary to trigger the reversal decreases to about 5 mT (Fig. 2c, region III). Furthermore, we find that the critical switching current scales with the lateral dimensions of the cobalt dot and the inverse pulse duration (Supplementary Information).

A systematic study of current-induced magnetization reversal as a function of applied field direction (Fig. 3) shows that the switching torque is maximal when **B** is applied parallel to **j** and decreases away from this orientation following a $\sin(\phi - \pi/2)$ function. Combining the above information, we observe that the action of the current on the magnetization is equivalent to that of an effective perpendicular magnetic field $\mathbf{B}_{Sz} \approx \mathbf{B}_R \times \mathbf{B} \approx (\hat{\mathbf{z}} \times \mathbf{j}) \times \mathbf{B}$, which changes sign on reversal of either **B** or **j** (Fig. 3c). In an FMM, however, relative to the internal exchange field produced by the local magnetization, the external field, **B**, has no direct influence on the spin polarization of the conduction electrons. Therefore, $\mathbf{B}_{Sz}$ shall be considered the perpendicular component of an effective magnetic field proportional to $\mathbf{B}_R \times \mathbf{M}$, where the orientation of **M** is initially determined by **B**.

Although there is no theory predicting the magnetization reversal mechanism reported here, we observe that there are at least two effects that can induce spin accumulation parallel to $\mathbf{B}_R \times \mathbf{M}$. We describe the first in analogy to phenomena observed in non-magnetic semiconductors. Faraday measurements performed on InGaAs heterostructures have shown that a magnetic field applied parallel to **j** induces a spin polarization component perpendicular to the plane of the current[11]. This phenomenon has been explained by the combined action of $\mathbf{B}_R$ and spin-dependent electron mobility, which leads to a net perpendicular spin accumulation proportional to the cross product $\mathbf{B}_R \times \mathbf{B}$ (ref. 12). We emphasize that this term has the same symmetry, current and field dependence as the effective switching field. This analogy suggests that a similar mechanism might be at work in our case, considering that the spin-dependent conductivity required to explain the effect in InGaAs is a common feature of FMMs[26]. Following this argument (see Supplementary Information for more details), the accumulation of out-of-plane spin polarization in an FMM requires a non-zero in-plane magnetization component parallel to **j**, induced by a small external field. The final effect, mediated by *s–d* exchange, is equivalent to that of a downward or upward effective field, $\mathbf{B}_{Sz}$, parallel to the *z* component of $\mathbf{B}_R \times \mathbf{M}$, in agreement with our measurements.

The second mechanism is based on the absorption of the spin current produced by the spin Hall effect (SHE) in platinum[13,14] and diffusing into the cobalt layer. The absorption of this current, polarized along the *y* direction, is equivalent to a torque acting on the cobalt magnetization that has the same symmetry as the effect reported here. Estimates based on the spin Hall angle in platinum, however, show that the SHE is not sufficient to account for the intensity of the switching field (Supplementary Information). Moreover, we find that samples with stronger PMA and a larger degree of aluminium oxidation switch more easily than do magnetically softer dots with equally thick cobalt and platinum layers (Supplementary Figs 8 and 9). This observation is not compatible with a simple explanation based on the SHE. Nevertheless, we cannot exclude either a partial contribution by the SHE to switching or a more complex mechanism involving the SHE. For example, the vertical gradient of the Rashba field at the cobalt–platinum interface might induce a supplementary spin current that adds to the SHE in platinum.

Although this work calls for a detailed theory of non-equilibrium spin–orbit phenomena in FMMs, it is important to distinguish two practical features of our results. First, when sufficient current and field are applied in the same direction, switching is robust and limited only by the intrinsic bistability of the FMM. Because neither the external field value nor its exact orientation is critical, a constant magnetic field produced by a macroscopic permanent magnet can be used to ensure

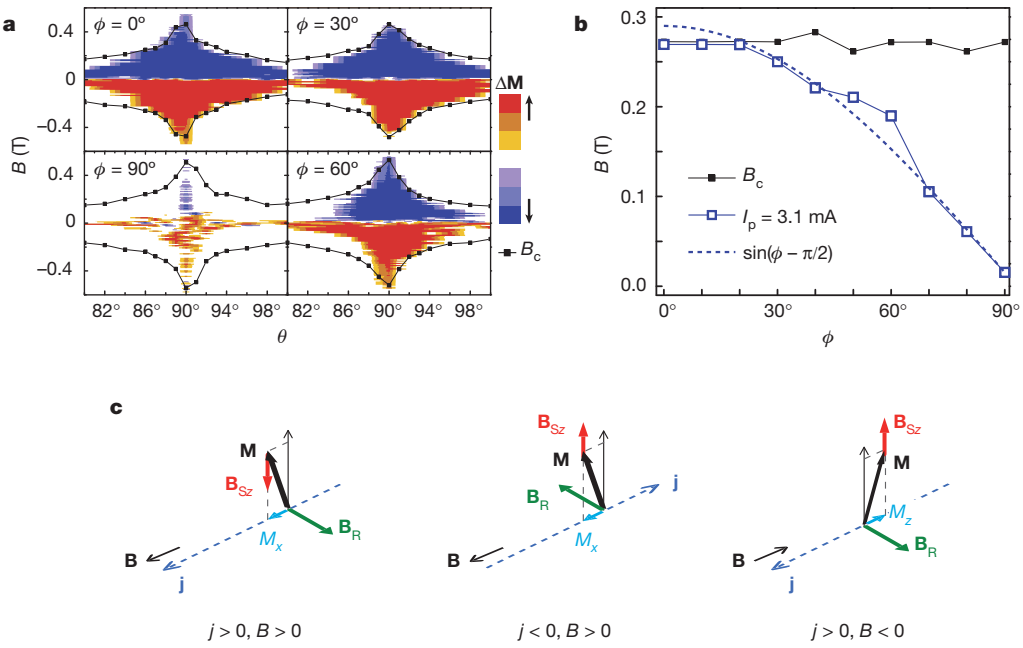

Figure 3 | Dependence of switching on applied field direction. **a**, Diagrams representing M_z reversal regions, showing the intensity and orientation of the applied magnetic field, **B**, at constant current ($I_p = 3.3$ mA). Colours indicate the switching sense: red, upwards; blue, downwards. Filled symbols show the coercive field at each angle. When **B** is aligned with the current ($\phi = 0°$), the switching areas extend throughout the entire bistability region delimited by B_c, with the exception of a narrow area near zero field. As **B** is rotated away from the current, the sizes of the switching areas gradually decrease. When **B** is perpendicular to the current ($\phi = 90°$), switching disappears and is replaced by random nucleation. **b**, Azimuthal dependence of the switching efficiency at constant current ($I_p = 3.1$ mA, $\theta = 87°$). Open symbols represent the largest field against which switching is observed; filled symbols show the coercive field. The dashed line is a sine function. **c**, Directions of the effective switching field, $\mathbf{B}_{Sz}$, relative to **j**, the in-plane magnetization component (M_x) induced by **B**, and the Rashba field, $\mathbf{B}_R$. The magnetization switches from 'up' to 'down' for $j > 0$, $B > 0$ and $j < 0$, $B < 0$, and from 'down' to 'up' for $j > 0$, $B < 0$ and $j < 0$, $B > 0$.

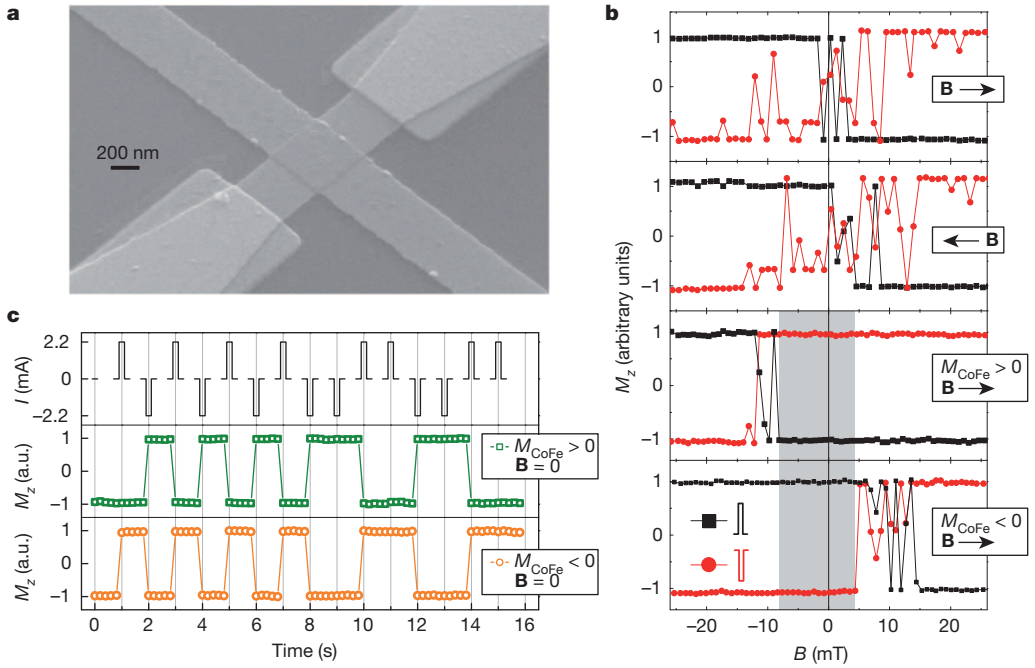

Figure 4 | Prototype of a reconfigurable ferromagnetic switch. **a**, Scanning electron micrograph of a device comprising two 50-nm-thick CoFe bar magnets parallel to the current injection line (bottom left and upper right corners) and an AlO_x–cobalt–platinum dot (centre). **b**, Top two panels: switching curve of a device without CoFe magnets around the zero field region. M_z is measured after injection of positive (black squares) and negative (red circles) pulses. No difference between positive and negative field sweeps is observed apart from random nucleation events near $B = 0$. Bottom two panels: switching curve of a device including on-chip magnets. The shaded areas show that bipolar switching extends to zero external field. Positive and negative field sweeps reveal the hysteretic behaviour of the CoFe magnets as well as the inversion of the switching polarity near $B = 0$. **c**, Controlled switching sequence of the device in zero field after setting positive (green squares) and negative (orange circles) CoFe magnetization. The switching current is $I_p = 2.5$ mA for pulses 9 ns long. a.u., arbitrary units.

bidirectional current switching of many independent magnetic bits. Second, the area separating the two opposite switching zones near $B = 0$ is very narrow, meaning that very small applied fields suffice to induce reversal. This feature prompts an approach for applications. Small permanent magnets can be fabricated on-chip, close to or on top of each active dot. In this way, not only can the dots be switched, but their response to the current direction can also be inverted by reversing the polarization of the magnets.

The ability to change the operation mode of a device is extremely valuable for programmable magnetic logic applications[27,28]. This motivated us to fabricate a small prototype switch by depositing two CoFe bars on top of the current injection lines near the cobalt dot (Fig. 4a). The shape anisotropy of the CoFe magnets ensures the alignment between their stray field and current lines. Figure 4b shows the low-field region of a typical switching curve, comparing results for a device without magnets (the two upper panels) with those of a device with CoFe bars (the two bottom panels). In the first case, as B approaches zero, switching is replaced by random nucleation events. In the second case, owing to the additional stray field of the magnets, the switching curve shows hysteretic behaviour extending to the zero-field region (shaded area). We further tested zero-field switching using a complex sequence of current pulses (Fig. 4c). After the magnetization of the CoFe magnets has been saturated in one of two opposite directions ($M_{CoFe} > 0$ and $M_{CoFe} < 0$), M_z reverses each time the pulses change polarity. As expected, reversing M_{CoFe} inverts the operation mode of the device.

The ability to switch a single magnetic layer at room temperature using an in-plane current opens the way to a new generation of spintronic devices, combining planar geometry, highly stable perpendicular magnetization, all-electrical write/read out schemes and reconfigurability. The layer structure of our prototype switch is extremely simple, is scalable and is based on materials compatible with present technology. The current density threshold for switching is of the order of 10^8 A cm^{-2}, and is expected to improve with further interface engineering. We note that, because the current is applied in-plane through a thin lateral surface, the absolute current required for switching can be made very small (<1 mA), providing significant gains in terms of integration and power consumption. Apart from its use in novel device architectures, this type of ferromagnetic switch also has interesting implications for existing technology. For example, a FMM oxide heterostructure could easily be integrated as the storage layer of a magnetic tunnel junction in magnetoresistive random-access memory, to decouple the read and write current paths. In this way, electrical stress of the tunnel barrier during the write process, which is an outstanding problem of the spin transfer approach[1,28], could be avoided while maintaining a large tunnel magnetoresistance and read-out sensitivity.

METHODS SUMMARY

The samples were fabricated from aluminium (1.6 nm), cobalt (0.6 nm) and platinum (3 nm) layers deposited on a thermally oxidized silicon wafer by d.c. magnetron sputtering[10]. The deposition rates were 0.05 nm s^{-1} (cobalt and aluminium) and 0.1 nm s^{-1} (platinum) at an argon pressure of 2×10^{-3} mbar. After deposition, the samples were oxidized by a 35-s exposure to radio-frequency oxygen plasma at a pressure of 3×10^{-3} mbar and a radio-frequency power of 10 W. This treatment ensures chemical stability of the layers and preserves the strong PMA typical of cobalt–platinum interfaces[10,29]. The presence of two dissimilar interfaces, of which one is a heavy metal characterized by strong spin–orbit coupling, gives rise to an electric potential gradient across the cobalt layer. This type of structure inversion asymmetry induces a Rashba-type magnetic field parallel to the y direction when the current flows along the x direction[9,30]. The AlO_x–cobalt–platinum films were patterned by electron beam lithography and ion beam etching into 500 nm × 500 nm AlO_x–cobalt dots and platinum Hall crosses (Methods). This geometry allows the magnetic state of the dots to be monitored by electric measurements using the anomalous Hall effect. If an electric current is applied along one arm of the cross, the Hall resistance, R_{Hall}, measured along the transverse arm, is proportional to the perpendicular component of the magnetization. Representative magnetization curves of a 500 nm × 500 nm device are shown in Supplementary Fig. 1. Smaller devices, 200 nm × 200 nm in size,

were fabricated to probe the scaling of the critical switching current with device size (Supplementary Fig. 5).

Full Methods and any associated references are available in the online version of the paper at www.nature.com/nature.

Received 14 February; accepted 16 June 2011.
Published online 31 July; corrected 11 August 2011 (see full-text HTML version for details).

1. Chappert, C., Fert, A. & Nguyen Van Dau, F. The emergence of spin electronics in data storage. *Nature Mater.* **6,** 813–823 (2007).
2. Ohno, H. *et al.* Electric-field control of ferromagnetism. *Nature* **408,** 944–946 (2000).
3. Chiba, D. *et al.* Magnetization vector manipulation by electric fields. *Nature* **455,** 515–518 (2008).
4. Myers, E. B., Ralph, D. C., Katine, J. A., Louie, R. N. & Buhrman, R. A. Current-induced switching of domains in magnetic multilayer devices. *Science* **285,** 867–870 (1999).
5. Ralph, D. C. & Stiles, M. D. Spin transfer torques. *J. Magn. Magn. Mater.* **320,** 1190–1216 (2008).
6. Chernyshov, A. *et al.* Evidence for reversible control of magnetization in a ferromagnetic material by means of spin–orbit magnetic field. *Nature Phys.* **5,** 656–659 (2009).
7. Moser, K. *et al.* Magnetic recording: advancing into the future. *J. Phys. D* **35,** R157–R167 (2002).
8. Batra, S. Hannay, J. D., Zhou, H. & Goldberg, J. S. Investigations of perpendicular write head design for 1 Tb/in^2. *IEEE Trans. Magn.* **40,** 319–325 (2004).
9. Miron, I. M. *et al.* Current-driven spin torque induced by the Rashba effect in a ferromagnetic metal layer. *Nature Mater.* **9,** 230–233 (2010).
10. Rodmacq, B., Manchon, A., Ducruet, C., Auffret, S. & Dieny, B. Influence of thermal annealing on the perpendicular magnetic anisotropy of Pt/Co/AlO$_x$ trilayers. *Phys. Rev. B* **79,** 024423 (2009).
11. Kato, Y. K., Myers, R. C., Gossard, A. C. & Awschalom, D. D. Current-induced spin polarization in strained semiconductors. *Phys. Rev. Lett.* **93,** 176601 (2004).
12. Engel, H.-A., Rashba, E. I. & Halperin, B. I. Out-of-plane spin polarization from in-plane electric and magnetic fields. *Phys. Rev. Lett.* **98,** 036602 (2007).
13. Ando, K. *et al.* Electric manipulation of spin relaxation using the spin Hall effect. *Phys. Rev. Lett.* **101,** 036601 (2008).
14. Liu, L., Moriyama, T., Ralph, D. C. & Buhrman, R. A. Spin-torque ferromagnetic resonance induced by the spin Hall effect. *Phys. Rev. Lett.* **106,** 036601 (2011).
15. Awschalom, D. & Samarth, N. Spintronics without magnetism. *Physics* **2,** 50 (2009).
16. Kato, Y., Myers, R. C., Gossard, A. C. & Awschalom, D. D. Coherent spin manipulation without magnetic fields in strained semiconductors. *Nature* **427,** 50–53 (2004).
17. Silov, A. Yu. *et al.* Current-induced spin polarization at a single heterojunction. *Appl. Phys. Lett.* **85,** 5929–5931 (2004).
18. Ganichev, S. D. *et al.* Electric current-induced spin orientation in quantum well structures. *J. Magn. Magn. Mater.* **300,** 127–131 (2006).
19. Stern, N. P. *et al.* Current-induced polarization and the spin Hall effect at room temperature. *Phys. Rev. Lett.* **97,** 126603 (2006).
20. Meier, L. *et al.* Measurement of Rashba and Dresselhaus spin–orbit magnetic fields. *Nature Phys.* **3,** 650–654 (2007).
21. Manchon, A. & Zhang, S. Theory of nonequilibrium intrinsic spin torque in a single nanomagnet. *Phys. Rev. B* **78,** 212405 (2008).
22. Garate, I. & MacDonald, A. H. Influence of a transport current on magnetic anisotropy in gyrotropic ferromagnets. *Phys. Rev. B* **80,** 134403 (2009).
23. Bychkov, Yu. A. & Rashba, E. I. Properties of a 2D electron gas with lifted spectral degeneracy. *J. Exp. Theor. Phys. Lett.* **39,** 78–81 (1984).
24. Krupin, O. *et al.* Rashba effect at magnetic metal surfaces. *Phys. Rev. B* **71,** 201403(R) (2005).
25. Tudosa, I. *et al.* The ultimate speed of magnetic switching in granular recording media. *Nature* **428,** 831–833 (2004).
26. Campbell, A. & Fert, A. in *Ferromagnetic Materials* Vol. 3 (ed. Wohlfart, E. P.) 747–803 (North Holland, 1982).
27. Ney, A., Pampuch, C., Koch, R. & Ploog, K. H. Programmable computing with a single magnetoresistive element. *Nature* **425,** 485–488 (2003).
28. Dieny, B. *et al.* Spin-transfer effect and its use in spintronic components. *Int. J. Nanotechnol.* **7,** 591–614 (2010).
29. Gambardella, P. *et al.* Giant magnetic anisotropy of single cobalt atoms and nanoparticles. *Science* **300,** 1130–1133 (2003).
30. Pi, U. H. *et al.* Tilting of the spin orientation induced by Rashba effect in ferromagnetic metal layer. *Appl. Phys. Lett.* **97,** 162507 (2010).

Supplementary Information is linked to the online version of the paper at www.nature.com/nature.

Acknowledgements We thank S. O. Valenzuela and S. F. Alvarado for reading the manuscript and for discussions. This work was supported by the European Research Council (StG 203239 NOMAD), the Ministerio de Ciencia y Innovación (ERA-Net EUI2008-03884, MAT2010-15659) and the Agència de Gestió d'Ajuts Universitaris i de Recerca (2009 SGR 695). Samples were patterned at the NANOFAB facility of the Institut Néel (CNRS).

Author Contributions I.M.M., K.G. and P.G. planned the experiment; I.M.M., G.G., P.-J.Z., M.V.C., S.A., S.B. and B.R. fabricated the samples; I.M.M. and K.G. performed the experiments; and I.M.M., K.G. and P.G. analysed the data and wrote the manuscript. All authors discussed the results and commented on the manuscript.

Author Information Reprints and permissions information is available at www.nature.com/reprints. The authors declare no competing financial interests. Readers are welcome to comment on the online version of this article at www.nature.com/nature. Correspondence and requests for materials should be addressed to I.M.M. (mihai.miron.icn@uab.es) and P.G. (pietro.gambardella.icn@uab.es).

METHODS

The samples were fabricated from aluminium (1.6 nm), cobalt (0.6 nm) and platinum (3 nm) layers deposited on a thermally oxidized silicon wafer by d.c. magnetron sputtering[10]. The deposition rates were 0.05 nm s^{-1} (cobalt and aluminium) and 0.1 nm s^{-1} (platinum) at an argon pressure of 2×10^{-3} mbar. After deposition, the samples were oxidized by exposure to radio-frequency oxygen plasma at a pressure of 3×10^{-3} mbar and a radio-frequency power of 10 W for 35 s. This treatment ensures chemical stability of the layers and preserves the strong PMA typical of cobalt–platinum interfaces[10,29]. The presence of two dissimilar interfaces, of which one is a heavy metal characterized by strong spin–orbit coupling, gives rise to an electric potential gradient across the cobalt layer. This type of structure inversion asymmetry induces a Rashba-type magnetic field parallel to the y direction when the current flows along the x direction[9,30].

Patterning. Square magnetic dots were patterned on top of the Hall cross by using two steps of electron beam lithography followed by ion beam milling and wet etching. During the first step, the current injection line is drawn onto the PMMA resist covering the AlO_x–cobalt–platinum layer. After development, 15 nm of titanium are deposited by electron beam evaporation. The lift-off procedure finally defines a 15-nm-thick titanium line. A second step of electron beam lithography (similar to the first one) is used to draw the transverse Hall branches perpendicular to the current injection line. Subsequently, we repeat the resist development, titanium evaporation and lift-off procedures. The device is now composed of two perpendicular, 15-nm-thick titanium lines that intersect. At their intersection, the total titanium thickness is 30 nm, the sum of the two depositions. Ion beam etching controlled by secondary ion mass spectroscopy is used to etch away the equivalent of 15 nm of titanium. At this stage, the AlO_x–cobalt–platinum layer is trimmed into a cross as the titanium mask has been removed everywhere except at the intersection of the two lines, where 15 nm of Ti remain unetched. We then used a chemically selective wet etching step to remove the oxide and the cobalt layers that are not covered by titanium. At the end of this process, the sample is composed of a platinum cross with a magnetic dot on top. The success of the fabrication technique is monitored by measurements of the anomalous Hall effect: after the chemical etching, the Hall resistance is reduced to approximately 70% of the initial value. The total device resistance was typically 3–5 kΩ. However, we note that most of the resistance drop occurs in the platinum current lines, which are 3 nm thick over a length of approximately 500 μm.

Electrical measurements. The current pulses were generated by a 100-V/2-A pulse generator (Agilent 8114A/001). The rise and fall times of the pulses were approximately 6 ns, as measured by a fast oscilloscope (Agilent DSO81304A) connected in series with the sample. The length of the current pulses was varied between 10 and 100 ns. We note that the pulse length was always longer than the characteristic timescale for magnetization dynamics (<1 ns) and that its effect is therefore analogous to that of a continuous current. To preserve the shape of the voltage pulse transmitted along the resistive platinum leads, we connected a 100-Ω resistance in parallel with the sample. Two 100-kΩ resistors were placed between the Hall branches and the data acquisition card (Fig. 1) to prevent current flow through the Hall contacts.